SCIENTIFIC REPORTS

OPEN

Nonlinear climatic sensitivity to greenhouse gases over past 4 glacial/interglacial cycles

Received: 7 February 2017
Accepted: 17 May 2017
Published online: 04 July 2017

Li Lo[1,2,3], Sheng-Pu Chang[1], Kuo-Yen Wei[1], Shih-Yu Lee[4], Tsong-Hua Ou[5], Yi-Chi Chen[1], Chih-Kai Chuang[1], Horng-Sheng Mii[6], George S. Burr[7], Min-Te Chen[8], Ying-Hung Tung[1], Meng-Chieh Tsai[1], David A. Hodell[2] & Chuan-Chou Shen[1]

The paleoclimatic sensitivity to atmospheric greenhouse gases (GHGs) has recently been suggested to be nonlinear, however a GHG threshold value associated with deglaciation remains uncertain. Here, we combine a new sea surface temperature record spanning the last 360,000 years from the southern Western Pacific Warm Pool with records from five previous studies in the equatorial Pacific to document the nonlinear relationship between climatic sensitivity and GHG levels over the past four glacial/interglacial cycles. The sensitivity of the responses to GHG concentrations rises dramatically by a factor of 2–4 at atmospheric CO_2 levels of >220 ppm. Our results suggest that the equatorial Pacific acts as a nonlinear amplifier that allows global climate to transition from deglacial to full interglacial conditions once atmospheric CO_2 levels reach threshold levels.

Rapidly rising anthropogenic CO_2 emissions over the past few decades pose a risk to human society and the biosphere. Relative to pre-industrial levels, the CO_2 concentration is projected to double to 560 ppm from 2050–2100, increasing the global mean temperature by 2.0–4.5 °C by the end of the 21st century. This warming is predicted to lead to large-scale ice sheet melting, shifts in rainfall patterns, and sea level rise[1]. Identifying the interactions among various forcing agents and feedback processes in the projected warming scenario is crucial to our understanding of social/biosystem sustainability and climate change mitigation strategies.

The tropical Pacific Ocean is the most important water vapor and moisture source to middle and high latitudes on the planet[2]. Accurately estimating tropical sea surface temperature (SST) responses to greenhouse gas (GHG)-induced radiative forcing (RF_{GHG}) is fundamental to reliable predictions. Past climate studies[3,4], however, assumed that the sensitivity of tropical ocean SST to atmospheric GHG content was linear. Physical model simulations were limited by a lack of pre-industrial observational records for climate transitions from low to high GHG levels. The energy budget of the global climate system is, therefore, difficult to precisely evaluate. This severely hinders our understanding of the mechanisms and energy interactions among climatic sub-systems.

The sensitivity of tropical Pacific Ocean SST to RF_{GHG}, mainly contributed by CO_2 and <5% by CH_4, during the past glacial/interglacial (G/IG) cycles was addressed[3–5]. Linear regression analyses[3,4,6] were conducted to evaluate the SST response to changes in pCO_2 assuming that the RF_{GHG} is the main driver of tropical SST and that the tropical Pacific SST would be 33–36 °C under a doubled CO_2 scenario. By comparing the atmospheric pCO_2 and SST values of the early Pleistocene to those of the late Pliocene, *Martinez-Boti et al.*[5] found a lower sensitivity under high atmospheric pCO_2 conditions, implying that the sensitivity may not respond linearly to the GHG level. Recent transient models[7] based on composite paleo-temperature records also revealed nonlinear sensitivity patterns since 800 thousand years ago (kyr BP, before 1950 AD). These variable responses to RF_{GHG} are supported

[1]High-Precision Mass Spectrometry and Environment Change Laboratory (HISPEC), Department of Geosciences, National Taiwan University, Taipei, 10617, Taiwan, ROC. [2]Department of Earth Sciences, University of Cambridge, Cambridge, Cambridgeshire, CB2 3EQ, UK. [3]State Key Laboratory of Isotope Geochemistry, Guangzhou Institute of Geochemistry, Chinese Academy of Sciences, Guangzhou, 510640, People's Republic of China. [4]Research Center for Environmental Changes, Academia Sinica, Taipei, 11529, Taiwan, ROC. [5]Institute of Applied Mechanics, National Taiwan University, Taipei, 10617, Taiwan, ROC. [6]Department of Earth Sciences, National Taiwan Normal University, Taipei, 11677, Taiwan, ROC. [7]NSF-Arizona Accelerator Mass Spectrometry Laboratory, University of Arizona, Tucson, AZ, 85721, USA. [8]Institute of Applied Geosciences, National Taiwan Ocean University, Keelung, 20224, Taiwan, ROC. Correspondence and requests for materials should be addressed to L.L. (email: lilo@gig.ac.cn) or S.-Y.L. (email: shihyu@gate.sinica.edu.tw) or C.-C.S. (email: river@ntu.edu.tw)

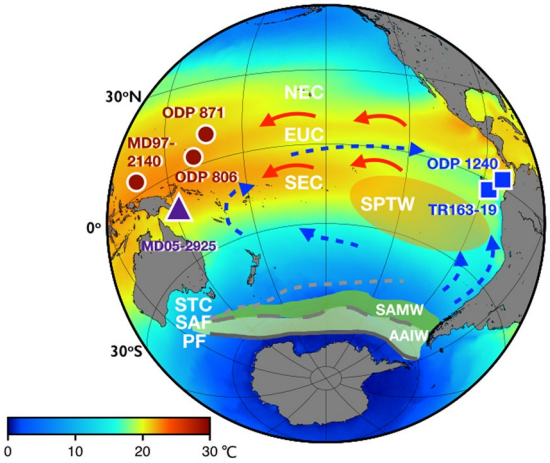

Figure 1. A sea surface temperature map with site locations, schematic circulation, and distribution of water masses. The purple triangle represents site MD05-2925. Dark red circles and blue squares are the selected sites in the equatorial Pacific. Gray solid, long dashed, and short dashed lines show the Polar Front (PF), Subantarctic Front (SAF), and Subtropical convergence zone (STC), respectively. Gray and green shadings denote the formation regions of Antarctic Intermediate Water (AAIW) and Subantarctic Mode Water (SAMW), respectively. Light orange shading represents the South Pacific Tropical Water (SPTW). Blue dashed arrays represent the undercurrent pathways of the Equatorial Under Current (EUC and water masses from southern ocean). Red solid arrows represent the surface South Equatorial Current (SEC) and North Equatorial Current (NEC). The AAIW and SAMW (gray and green shadings) flow from the southern hemisphere high latitudes to the SPTW region and spread out to the South Pacific Ocean through the EUC and EEP wind-driven upwelling system and resurfacing processes through water mass mixing on the scale of decades[20]. This map was generated with Generic Mapping Tools (GMT) version 5 (ref. 40). Global satellite mean annual sea surface temperatures during 2009–2013 with color coding are from the National Aeronautics and Space Administration (NASA) Ocean Color database (http://oceancolor.gsfc.nasa.gov)[41].

by a conceptual and dynamic-flow box modeling study[8] that argues for the existence of possible step-wise and/or different equilibrium climate states during G/IG cycles.

This dispute, linear versus nonlinear climatic sensitivities, hinders our understanding of climate evolution and our ability to evaluate the fidelity of global energy simulations under the current warming stress. Orbital-scale high-resolution SST records are required to clarify this debate. Here, we combine a new record of southern Western Pacific Warm Pool (WPWP) SST anomalies (ΔSST) and previously published equatorial Pacific records[4,9–11] for the past four G/IG cycles to document the non-linearity of the relationship between equatorial Pacific SSTs and GHG levels and to identify the specific pCO_2 threshold.

A marine sediment core, MD05-2925 (9.3°S, 151.5°E, water depth 1661 m), was retrieved from the Solomon Sea east of Papua New Guinea (Figs 1, S1). The age model for MD05-2925 was established using radiocarbon dates[12] and composite benthic foraminiferal oxygen isotopic stratigraphy (Figs S2, S3). The Mg/Ca ratios of planktonic foraminifera, *Globigerinoides ruber*, were determined using a sector field inductively coupled plasma mass spectrometer (SF-ICP-MS)[13] and were used to establish a 360-kyr SST sequence with 200- to 900-year resolution.

Results

Foraminiferal Mg/Ca-inferred Solomon Sea SST. The new reconstructed Solomon Sea SST record shows a large G/IG change of approximately 4 °C, which is supported by a previous study[14] (Fig. 2a). The interglacial temperatures of 28–29 °C during Marine Isotope Stage (MIS) 7 and MIS 9 are similar to those of the Holocene and are higher by 1–2 °C than those of MIS 5. Large SST variations of 2–3 °C can be observed during glacial periods, such as MIS 2–4, 6 and 8.

Spectral analysis (Fig. S5) shows that the Solomon Sea SST record is characterized by strong obliquity pacing and a good correlation with Antarctic temperature changes during the past four G/IG cycles. The Southern Hemisphere (SH) middle- to high-latitude climate apparently exerts a significant influence on the Solomon Sea, possibly by oceanic tunnel connections[11,12] (Figs S5–S9).

The statistical correlation shown in Figure S7 suggests that the SST changes in the Solomon Sea could be related to SH high-latitude climate variation, similar to the eastern equatorial Pacific (EEP) upwelling region[11]. The trends in the time series of Antarctic temperature and southern WPWP SST have been similar since 360 ka ($R^2 = 0.59$ or 0.65 if MIS 7 is omitted, Fig. S7). This correlation implies a persistent teleconnection between the two regions (Figs S7–S9)[12]. Therefore, the southern WPWP and EEP regions are linked to Southern Ocean climate and/or affected directly by the RF_{GHG}[3,15,16].

Climate sensitivity and regional comparisons. The relationship between tropical ΔSST and the atmospheric RF_{GHG} anomaly (relative to pre-industrial levels, ΔRF_{GHG}) for the Solomon Sea record is plotted in Figure 3. This comparison expresses a striking nonlinear correlation with a significant change at an atmospheric

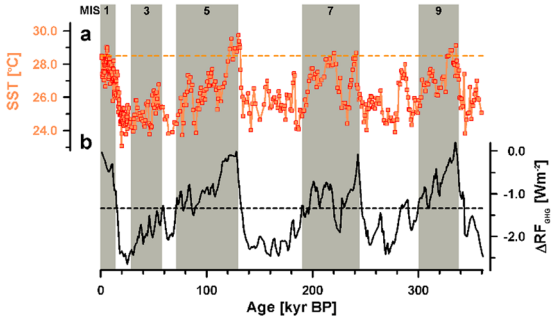

Figure 2. MD05-2925 SST values and ΔRF_{GHG} of greenhouse gases. (**a**) Mg/Ca-inferred SST in the Solomon Sea. (**b**) Calculated ΔRF_{GHG} (see Methods). Gray bars indicate interglacial periods. The orange and black dashed lines are the modern annual average SST (28.5 °C) and the $CO_2 = 220$ ppm, respectively.

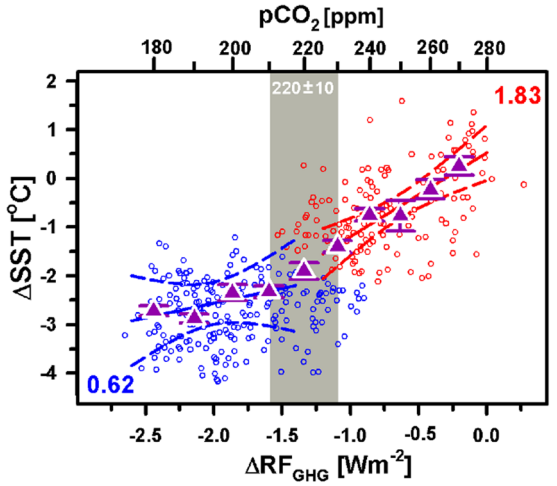

Figure 3. Nonlinearity of SST sensitivity to climate in the southern WPWP. The Solomon ΔSST and greenhouse gas radiative forcing ΔRF_{GHG} data are plotted at a 1-kyr interval. Two groups (blue and red circles) were divided at a pCO_2 level of 220 ppm via cluster analysis (see Methods). Purple triangles are standard deviations of the mean for ΔSST data points at a segment of radiative forcing corresponding to 10 ppm pCO_2. Solid and dashed lines for each group represent the regression line and 95% confidence interval, respectively. The determined slopes are given as lines. The gray vertical bar marks the significant difference threshold for the non-linear SST changes at a pCO_2 level of 220 ± 10 ppm.

CO_2 threshold of 220 ± 10 ppm (Fig. 3). Southern WPWP ΔSST values increase from -4.1 to -1.2 °C as the ΔRF_{GHG} values increase from -2.75 to -1.55 W m^{-2}, corresponding to a pCO_2 range of 170–210 ppm. Thus, the sensitivity is 0.62 ± 0.33 °C (W m^{-2})$^{-1}$. Note that all the sensitivity uncertainties are given in 1σ range (Table S3). During the second interval, ΔRF_{GHG} increases from -1.55 to 0 W m^{-2} (210–280 ppm pCO_2). The sensitivity increases to 1.83 ± 0.17 °C (W m^{-2})$^{-1}$ as ΔSST increases from -2.1 to 1.8 °C. No significant differences are observed in the SST-RF_{GHG} response among the past four G/IG periods at 1–70, 71–160, 161–270, and 271–360 kyr BP (Fig. S8), indicating that the correlation is independent of the G/IG cycles in this region.

A comparison of ΔSST and pCO_2 values over the past 3–4 G/IG cycles at six western and eastern equatorial Pacific sites (Fig. 1) is shown in Figure 4. Five (MD05-2925, ODP 1240, TR163-19, MD97-2140, and ODP 871) of the six sites are characterized by a nonlinear SST-RF_{GHG} relationship with an atmospheric CO_2 threshold of 220 ± 10 ppm (Fig. 4). Comparable to the southern WPWP site MD05-2925, the SH-affected EEP upwelling sites of ODP 1240 and TR163-19 also feature similar nonlinearity. Sites ODP 1240 and TR163-19 have low sensitivities of 0.61 ± 0.14 and 0.51 ± 0.14 °C (W m^{-2})$^{-1}$, respectively, at pCO_2 values of $<220 \pm 10$ ppm and high sensitivities of 2.35 ± 0.17 and 1.29 ± 0.50 °C (W m^{-2})$^{-1}$, respectively, at pCO_2 values of $>220 \pm 10$ ppm. A similar nonlinearity was also reported in the southern WPWP region over the past 400 kyr BP (Fig. 5 of ref. 15).

MD97-2140, ODP 871, and ODP 806 in the northern WPWP show more complicated patterns. MD97-2140 and ODP 871 have nonlinear relationships and sensitivities of -0.20 ± 0.15 to 1.01 ± 0.57 °C (W m^{-2})$^{-1}$, respectively, which are less than the values of the EEP sites and MD05-2925. ODP 806 is the only site characterized by a linear trend due to an absence of statistics-based different sensitivities (Table S3). Its sensitivity is 0.70 ± 0.10 °C (W m^{-2})$^{-1}$ (Fig. 4). The nonlinearity observed in the northern WPWP can be attributed to equatorial upwelling, regional oceanic dynamics, and topographic settings[4], which might transport high latitude climatic effects to equatorial Pacific[17,18].

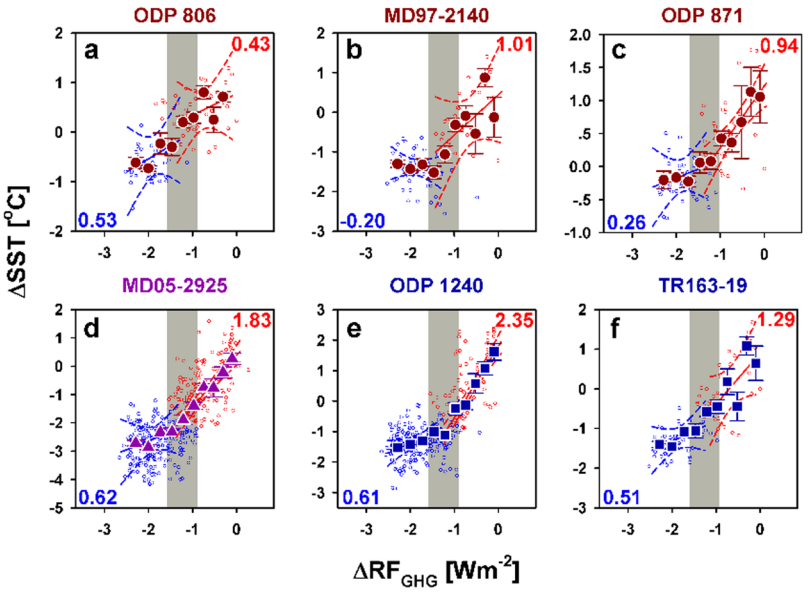

Figure 4. Comparison of tropical Pacific SST sensitivities. (**a**–**c**) Western Pacific with three sites: ODP 806, MD97-2140, and ODP 871 (refs 4, 9, 10). (**d**) Solomon Sea (site MD05-2925, this study). (**e**,**f**) Eastern equatorial Pacific with two sites: ODP 1240 and TR163-19 (refs 9, 11). Symbols, lines, slopes, and gray vertical bars are the same as in Figure 3 but for multiple sites. The data from three G/IG cycles are used in (**e**), and data from four G/IG cycles are used in the other panels.

Discussion

We hypothesize that this general nonlinear SST response is associated with the sea ice coverage in the Southern Ocean, the related release of ocean-derived CO_2, and induced atmospheric radiative forcing during the last four G/IG cycles. *Jaccard et al.*[19] presented sedimentary evidence that sea ice in the Southern Ocean could affect oceanic-atmospheric CO_2 exchange by controlling the Subarctic Mode Water (SAMW) and Antarctic Intermediate Water (AAIW) formations during the past one million years. The SH high-latitude impact on the equatorial Pacific hydroclimate and the teleconnection between SAMW/AAIW and South Pacific Tropical Water (SPTW, Fig. 1) have been reported based on evidence from the subtropical gyre and resurfacing processes, such as upwelling and mixing[20]. The oceanic tunneling process represents the link between the Southern Ocean modulation and the WPWP and EEP. The possible processes are as follows. The gradual melting of sea ice in the Subantarctic Zone and the release of CO_2 during the initial phase of glacial termination could cause the first stage of the SST-RF_{GHG} response. Positive latent and sensible heating likely then triggers a sudden retreat of Southern Ocean sea ice and a rapid increase in pCO_2, leading to warming and a better ventilated SAMW/AAIW[21]. A pCO_2 level of 220 ± 10 ppm can be considered the critical threshold for runaway melting and is supported by an Earth system model simulation[22].

Our hypotheses are supported by previous climate reconstructions[23,24]. Taking the last termination as an example, a pCO_2 level of 220 ± 10 ppm occurred during Heinrich event 1, when meridional circulation shut down, the Southern Ocean warmed, and releases from the major deep-sea carbon reservoir began[23]. Benthic foraminiferal $\delta^{13}C$ and SST data from the southwestern Pacific also suggest that the SAMW/AAIW experienced periods of relatively strong and weak ventilation[24].

The responses of the WPWP and EEP thermal conditions to GHGs imply that the Southern Ocean–tropical ocean link acts as a nonlinear amplifier during glacial terminations via ocean circulation and atmospheric energy feedbacks. Once the pCO_2 level exceeded 220 ppm, the southern WPWP SSTs increased by 1.83 °C $(W\ m^{-2})^{-1}$, a rate that is three times higher than that associated with pCO_2 levels of <220 ppm. The higher SST and increased latent heating may also have acted as a positive feedback mechanism, contributing to the collapse of high-latitude ice sheets[25]. Rapid warming in the equatorial Pacific possibly further weakened Hadley circulation[12] and strengthened the SH westerlies. The enhanced Southern Ocean upwelling was then able to release more CO_2 into the atmosphere[23]. Similar climatic threshold behavior during the past one million years of G/IG oscillations has been reported[19]. The teleconnection between the southern and northern hemisphere climates via WPWP and EEP SSTs during past G/IG cycles suggests that the tropical climate system plays a crucial role in rapid climatic transitions on Earth.

The clear relationship between equatorial Pacific SSTs and RF_{GHG} provides an important reference for understanding past and future climate dynamics. First, the mechanism that controls the nonlinearity in different oceans needs to be confirmed to improve predictions of the responses to increases in pCO_2. Second, the potential existence of another higher CO_2 threshold should be determined. *Martinez-Boti et al.*[5] reported that the climate sensitivity could be similar or greater at higher pCO_2 levels. The spatial variability in climate sensitivity during the Pliocene, with pCO_2 levels of 300–500 ppm, remains unknown. More spatial and temporal high-resolution SST records and accurate GHG concentration reconstructions are required to clarify the complexity of the tropical

ocean thermal response to RF_{GHG} changes and potential high-latitude teleconnections and to understand the linkages between tropical and high-latitude climate systems at different timescales.

Methods

Site MD05-2925. A marine sediment core was obtained at site MD05-2925 during the 2005 PECTEN (Past Equatorial Climate: Tracking El Niño) cruise, which was supported by the International Marine and Climate Changes (IMAGES) Project, on the research vessel Marion Dufresne. This site is located on the Woodlark rise, Solomon Sea, which is close to Papua New Guinea (PNG). The main route of the South Equatorial Current (SEC) traverses the Solomon Sea. The SEC originates in the mid-latitudes and travels to the equator. The annual average SST is 28.5 °C (ref. 26) and the seasonal variations are from 27.4 to 29.4 °C from the closest observational site at 8°S (ref. 27).

Age model. The MD05-2925 age model was established using accelerator mass spectrometry radiocarbon (AMS ^{14}C) dates and benthic foraminiferal oxygen isotope stratigraphic correlation. The compiled benthic foraminiferal $\delta^{18}O$ data were correlated to the global benthic foraminiferal $\delta^{18}O$ stack (LR04, ref. 28) (Figs S2, S3). All benthic foraminiferal tests were >250 μm in size, and 2–5 tests were used to measure $\delta^{18}O$ values. Our group has reported the first 282-kyr age model[12,29] and adopt the interspecies $\delta^{18}O$ offset constants from previous studies[29]. All oxygen isotope age control points are summarized in Table S1.

Planktonic foraminiferal $\delta^{18}O$ and Mg/Ca ratio. In total, 40–60 planktonic foraminifera *G. ruber* (white, *s.s.*, 250–300 μm) were picked for oxygen isotopic measurements and Mg/Ca determinations. Each of the paired $\delta^{18}O$-Mg/Ca measurements, 20–30 tests were crashed and mixed for clearing procedure. For the oxygen isotope measurements, the samples were ultrasonicated 3–4 times, immersed in NaOCl for 24 hours, and dried. The cleaned samples were measured using an isotope ratio mass spectrometer (IRMS) at the National Taiwan Normal University. Analytical reproducibility is ±0.60‰ (2 RSD, N = 701)[12] with respect to the Vienna Pee Dee Belemnite (VPDB). For the Mg/Ca measurements, the shells were gently crushed and placed in Teflon vials. The cleaning procedure followed that of *Lo et al.*[13]. Cleaned samples were dissolved in 5% HNO_3 and measured using a Thermo-Finngan Element II sector field inductive coupled plasma mass spectrometer (SF-ICP-MS) at the High-Precision Mass Spectrometry and Environment Change Laboratory (HISPEC), Department of Geosciences, National Taiwan University. The external uncertainty is ± 0.60% (2 RSD). *G. ruber* $\delta^{18}O$ and Mg/Ca values during the last termination (23-10 kyr BP) were previously reported[12].

SSTs inferred from *G. ruber* Mg/Ca ratios. The average Solomon Sea *G. ruber* Mg/Ca ratios vary from approximate 3.5 mmol mol^{-1} during the glacial periods to 4.5–5.0 mmol mol^{-1} during the interglacial periods (Fig. S4b). We adapted composite equation $Mg/Ca = 0.38 \times e^{(0.09 \times SST)}$ to calculate the corresponding SST values[30,31]. The average *G. ruber* shell weight during glacial periods (11.37 ± 1.11 μg, 1RSD, n = 20) does not differ from that during interglacial periods (11.46 ± 0.78 μg, 1RSD, n = 21) (Fig. S4d). The coarse fraction weight percentage shows no clear G/IG changes, which is reported to be linked with the carbonate preservation condition in the eastern equatorial Pacific region[32] (Fig. S4c). Accordingly, no additional dissolution correction needs to be applied to the MD05-2925 Mg/Ca ratios, similar to the SST record reported in the northern PNG region[15].

ΔRF_{GHG} calculation. We reconstructed ΔSST (Eq. 1) and ΔRF_{GHG} (Eq. 2) by referencing the measured SSTs from the marine sediment core and the content of EPICA ice core greenhouse gases to the modern value.

$$\Delta SST = SST_i - SST_0 \tag{1}$$

ΔSST is defined as the difference between past temperatures (SST_i) and the modern annual average temperature (SST_0, 28.5 °C)[26]. ΔRF_{GHG} is defined as the difference between a certain past GHG level ($[CO_2]$ and $[CH_4]$) and the pre-industrial greenhouse gas level ($[CO_2]_0 = 280$ ppm, $[CH_4]_0 = 700$ ppb)[33]. Although CH_4 contributes only <5%, we calculated the ΔRF_{GHG} using both CO_2 and CH_4. The negative feedback from N_2O is negligible with respect to RF[26]. The equation used to determine ΔRF_{GHG} is as follows:

$$\begin{aligned}\Delta RF_{GHG} &= \Delta RF_{CO2} + \Delta RF_{CH4} \\ &= 4.841 \ln([CO_2]/[CO_2]_0) + 0.0906(\sqrt{[CO_2]} - \sqrt{[CO_2]_0} \\ &+ 0.036 \ln(\sqrt{[CH_4]}) - (\sqrt{[CH_4]_0}).\end{aligned} \tag{2}$$

Regional sensitivity comparison. We summarized the updated *G. ruber* Mg/Ca records, which included at least three G/IG cycles, and calculated the relationships between ΔSST and ΔRF_{GHG}. The records of ODP 806 (0.3°N, 159.4°E, water depth 2520 m)[9], MD97-2140 (2.0°N, 141.7°E, water depth 2547 m)[10], ODP 871 (5.6°N, 172.3°E, water depth 1255 m)[4], TR163-19 (2.3°N, 91°W, water depth 2348 m)[9], and ODP 1240 (0.0°N, 86.5°E, water depth 2921 m)[11] were used. The Mg/Ca records of ODP 806 and TR163-19 have been recently calibrated using the dissolution correction equation[4]. We resampled ODP 806, ODP 871, TR163-19, and MD97-2140 at a 4-kyr interval and ODP 1240 at a 1-kyr interval and compared them to the contemporaneous resampled Antarctica ΔT and pCO_2 records with the AICC2012 age model[34,35], following the methods of previous studies[4,9]. No significant lead-lag difference is observed between the Antarctic and Solomon Sea ΔSST records (Table S2).

Statistical methods to identify nonlinearity. *Non-overlapping binned method.* A non-overlapping binned method, used by the compilation of tropical SSTs (ref. 12), was applied to calculate the average trend

of ΔSST versus ΔRF_{GHG}. A radiative forcing window corresponding to 10 ppm pCO_2 was used to calculate the average value of ΔSST and standard deviation of the mean for each of the SST data locations with different time resolutions.

Cluster analysis. K-means clustering analysis[36] is widely used in diverse fields[37–39] to statistically determine inflection points from separated k groups of any dataset with a non-linear trend. The data shown in all panels of Figures 3 and 4 were divided into two groups by k-means analysis. The regression lines with a 95% confidence interval of the two groups were calculated.

References

1. IPCC AR5 report. Contribution of Working Groups I, II and III to the Fifth Assessment Report of the Intergovernmental Panel on Climate Change. Core Writing Team, Pachauri, R.K. and Reisinger, A. (Eds). IPCC, Geneva, Switzerland. pp. 104 (2014).
2. Cane, M. A. A role for the tropical. *Pacific. Science* **282**, 59–61 (1998).
3. Lea, D. W. The 100,000-yr cycle in tropical SST, greenhouse forcing, and climate sensitivity. *J. Clim.* **17**, 2170–2179 (2004).
4. Dyez, K. A. & Ravelo, A. C. Late Pleistocene tropical Pacific temperature sensitivity to radiative greenhouse gas forcing. *Geology* **41**, 23–26 (2012).
5. Martinez-Boti, M. A. *et al.* Plio-Pleistocene climate sensitivity evaluated using high resolution CO_2 records. *Nature* **518**, 49–54 (2015).
6. MacDougall, A. H. The transient response to cumulative CO_2 emissions: a review. *Curr. Clim. Change Rep* **2**, 39–47 (2016).
7. Friedrich, T., Timmernmann, A., Tigchelaar, M., Timm, O. E. & Ganopolsji, A. Nonlinear climate sensitivity and its implications for future greenhouse warming. *Sci. Adv* **2**, e1501923 (2016).
8. Carlson, A. E. & Winsor, K. Northern Hemisphere ice-sheet responses to past climate warming. *Nat. Geosci.* **5**, 607–613 (2012).
9. Lea, D. W., Pak, D. K. & Spero, H. J. Climate Impact of Late Quaternary Equatorial Pacific Sea Surface Temperature Variations. *Science* **298**, 1719–1724 (2000).
10. de Garidel-Thoron, T., Rosenthal, Y., Bassinot, F. & Beaufort, L. Stable sea surface temperatures in the western Pacific warm pool over the past 1.75 million years. *Nature* **433**, 294–298 (2005).
11. Pena, L. D., Cacho, I., Ferretti, P. & Hall, M. A. El Niño-Southern Oscillation-like variability during glacial terminations and interlatitudinal teleconnections. *Paleoceanography* **23**, PA3101 (2008).
12. Lo, L. *et al.* Millennial meridional dynamics of the Indo-Pacific Warm Pool during the last termination. *Clim. Past* **10**, 2253–2261 (2014).
13. Lo, L. *et al.* Determination of element/Ca ratios in foraminifer and coral using cold- and hot-plasma techniques on inductively coupled plasma sector field mass spectrometry. *J. Asian Earth Sci.* **81**, 115–122 (2014).
14. Tripati, A. K. *et al.* Modern and glacial tropical showlines controlled by sea surface temperature and atmospheric mixing. *Nat. Geosci.* **7**, 205–209 (2014).
15. Tachikawa, K., Timmermann, A., Vidal, L., Sonzogni, C. & Timm, O. E. CO_2 radiative forcing and Intertropical Convergence Zone influences on western Pacific warm pool climate over the past 400 ka. *Quat. Sci. Rev.* **86**, 24–34 (2014).
16. Shakun, J. D., Lea, D. W., Lisiecki, L. E. & Raymo, M. E. An 800-kyr record of global surface ocean $\delta^{18}O$ and implications for ice volume-temperature coupling. *Earth Planet. Sci. Lett.* **426**, 58–68 (2015).
17. Goodman, P. J., Hazeleger, W., de Vries, P. & Cane, M. Pathyways into the Pacific Equatorial Undercurrent: A trajectory analysis. *J. Phys. Oceano* **35**, 2134–2151 (2005).
18. Lee, S.-Y. & Poulsen, C. J. Tropical Pacific climate response to obliquity forcing in the Pleistocene. *Paleoceaography* **20**, PA4010, doi:10.1029/2005PA001161 (2005).
19. Jaccard, S. L. *et al.* Two modes of change in Southern Ocean productivity over the past million years. *Science* **339**, 1419–1423 (2013).
20. Qu, T., Gao, S. & Fine, R. A. Subduction of South Pacific tropical water and its equatorward past way shown by a simulated passive tracer. *J. Phys. Oceanogr.* **43**, 1551–1656 (2013).
21. Sigman, D. M., Hain, M. P. & Haug, G. H. The polar ocean and glacial cycles in atmospheric CO_2 concentration. *Nature* **466**, 47–55 (2010).
22. Abe-Ouchi, A. *et al.* Insolation-driven 100,000-year glacial cycles and hysteresis of ice-sheet volume. *Nature* **500**, 190–193 (2013).
23. Anderson, R. F. *et al.* Wind-driven upwelling in the Southern Ocean and the deglacial rise in atmospheric CO_2. *Science* **323**, 1443–1448 (2009).
24. Pahnke, K., Zahn, R., Elderfield, H. & Schulz, M. 340,000-year centennial-scale marine record of Southern Hemisphere climatic oscillation. *Science* **301**, 948–952 (2003).
25. Clark, P. U., Hostetler, S. W., Pisias, N. G., Schmittner, A. & Meissner, K. J. Mechanism for a ~7-kyr climate and sea-level oscillation during marine isotope stage 3, in *Ocean Circulation: Mechanisms and Impacts*, A. Schmittner, J. Chiang, S. Hemming, Eds Geophysical Monograph 173, American Geophysical Union, Washington, DC, pp. 209–246 (2007).
26. Locarnini, R. *et al.* World Ocean Atlas 2009, in Levitus, S. ed. *NOAA Atlas NESDIS 68*, U.S. Government Printing Office, Washington, D.C. (2010).
27. Delcroix, T. *et al.* Sea surface temperature and salinity seasonal changes in the western Solomon and Bismarck Seas. *J. Geophys. Res. Oceans* **119**, 2642–2657 (2014).
28. Lisiecki, L. E. & Raymo, M. E. A Pliocene-Pleistocene stack of 57 globally distributed benthic $\delta^{18}O$ records. *Paleoceanography* **20**, PA1003 (2005).
29. Liu, Y. *et al.* Obliquity pacing of the western Pacific Intertropical Convergence Zone over the past 282,000 years. *Nat. Commun.* **6**, doi:10.1038/ncomms10018 (2015).
30. Anand, P., Elderfield, H. & Conte, M. H. Calibration of Mg/Ca thermometry in planktonic foraminifera from a sediment trap time series. *Paleoceanography* **18**, PA1050 (2003).
31. Dekens, P. S., Lea, D. W., Pak, D. K. & Spero H. J. Core top calibration of Mg/Ca in tropical foraminifera: Refining paleotemperature estimation. *Geochem. Geophy. Geosys.* **3**, doi:10.1029/2001GC000200 (2002).
32. Lalicata, J. J. & Lea, D. W. Pleistocene carbonate dissolution fluctuations in the eastern equatorial Pacific on glacial timescales: Evidence from ODP Hole 1241. *Mar. Micropaleo* **79**, 41–51 (2011).
33. Ramaswamy, V. *et al.* Radiative forcing of climate change in, *Climate Change 2001: The Scientific Basis*, Houghton, J. T. *et al.* eds, Cambridge University Press, 319–416 (2001).
34. Bazin, L. *et al.* An optimized multi-proxy, multi-site Antarctic ice and gas orbital chronology (AICC2012): 120–800 ka. *Clim. Past* **9**, 1715–1731 (2013).
35. Veres, D. *et al.* The Antarctic ice core chronology (AICC2012): an optimized multi-parameter and multi-site dating approach for the last 120 thousand years. *Clim. Past* **9**, 1733–1748 (2013).
36. Hartigan, J. A. & Wong, M. A. Algorithm AS 136: A k-means clustering algorithm. *J. R. Stat. Soc* **28**, 100–108 (1979).
37. Cosimo, S., Vinka, B., Pierluigi, B. Gianpiero, C. & Serena, F. U. Understanding dynamic of biogeochemical properties in the northern Adriatic Sea by using self-organizing maps and k-means clustering. *J. Geophy. Res. Oceans* **112**, doi:10.1029/2006JC003553 (2007).

38. Martins, D. S., Raziei, T., Paulo, A. A. & Pereira, L. S. Spatial and temperoal variability of precipitation and drought in Portugal. *Nat. Hazards Earth Syst. Sci.* **12**, 1493–1501 (2012).
39. Loikith, P. C. *et al*. Classifying reanalysis surface temperature probability density functions (PDFs) over North America with cluster analysis. *Geophy. Res. Lett* **40**, 3710–3714 (2013).
40. Wessel, P., Smith, W. H. F., Scharroo, R., Luis, J. F. & Wobbe, F. Generic Mapping Tools: Improves versions released. *EOS Trans. AGU* **94**, 40–410 (2013).
41. NASA Ocean Biology (OB.DAAC). Mean annual sea surface temperature for the period 2009–2013. http://data.unep-wcmc.org/datasets/36 (2014).

Acknowledgements

The authors would like to thank the chief scientists Luc Beaufort and Min-Te Chen of the 2005 PECTEN cruise, which was supported by the IMAGES group. This project was supported by Taiwan ROC MOST (104-2119-M-002-003, 104-2917-I-564-046, 105-2119-M-002-001, 105-2116-M-002-026-MY3), National Taiwan University (105R7625), State Key Laboratory of Isotope Geochemistry, Guangzhou Institute of Geochemistry, Chinese Academy of Sciences (SKLaBIG-QD-16-04) and Academia Sinica.

Author Contributions

C.-C.S. directed the project. L.L., S.-Y.L., K.-Y.W., and C.-C.S., prepared the manuscript. S.-P.C. and L.L. measured planktonic foraminiferal Mg/Ca ratios. T.-H.O. and L.L. conducted statistics analyses. Y.-C.C., C.-K.C., L.L. and H.-S.M. measured planktonic and benthic foraminiferal $\delta^{18}O$ and established the age model. G.S.B. helped with ^{14}C dating. Taiwan Ocean Research Institute provided sediment material. Y.-H.T. and M.-C.T. calculated radiative forcing and made figures. All authors revised and improved the manuscript.

Additional Information

Supplementary information accompanies this paper at doi:10.1038/s41598-017-04031-x

Competing Interests: The authors declare that they have no competing interests.

Publisher's note: Springer Nature remains neutral with regard to jurisdictional claims in published maps and institutional affiliations.